Title

Comparative tissue proteomics reveals unique action mechanisms of vaccine adjuvants.

Journal

iScience, 26(1)

Authors

Li, Yibo

Li, Zhuofan

Chen, Xinyuan

Publication Date

2023-01-20

DOI

10.1016/j.isci.2022.105800

Peer reviewed

iScience

CellPress
OPEN ACCESS

Article

Comparative tissue proteomics reveals unique action mechanisms of vaccine adjuvants

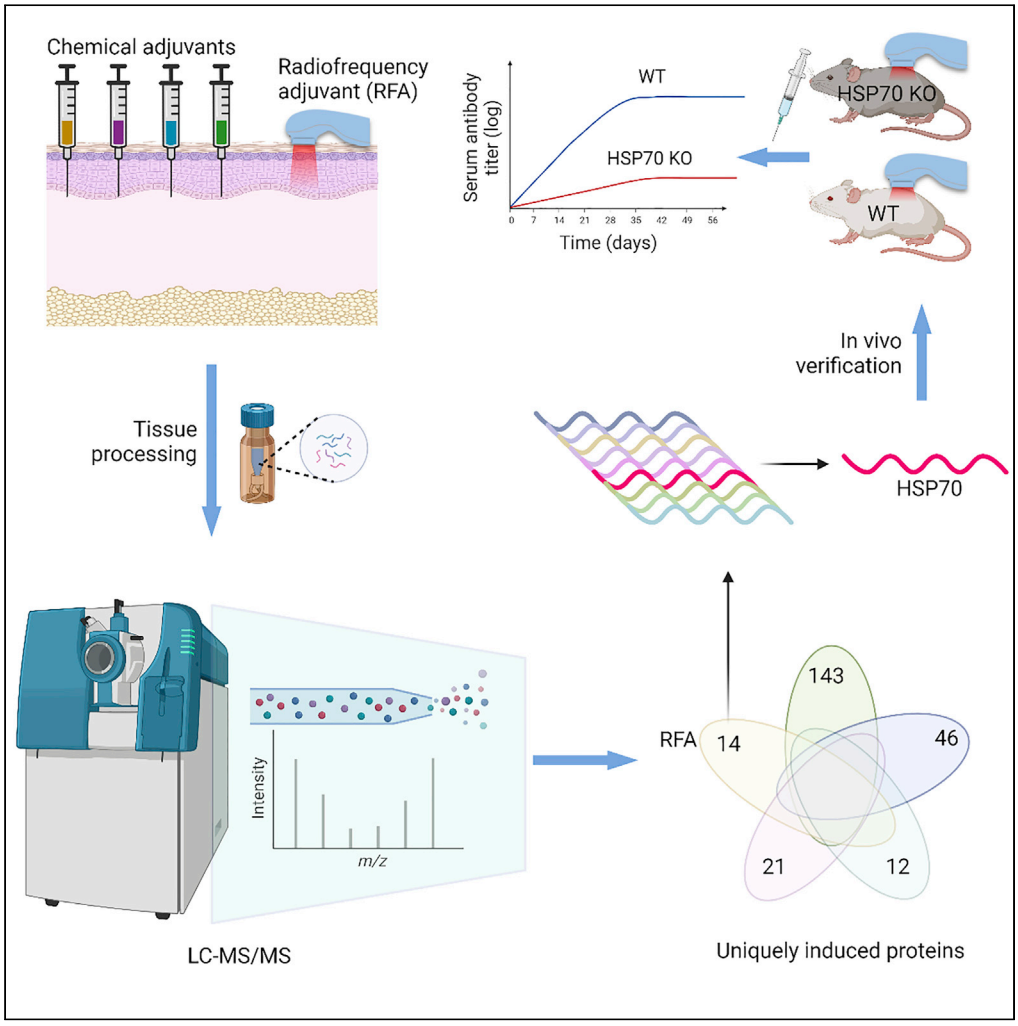

Yibo Li, Zhuofan Li, Xinyuan Chen

xchen14@uri.edu

Highlights

Comparative tissue proteomics identified uniquely induced proteins by adjuvants

MF59-mimetic AddaVax adjuvant showed the most impact on local tissue proteome

Radiofrequency adjuvant showed the least impact on local tissue proteome

HSP70 was identified as a key player in radiofrequency adjuvant effects

Li et al., iScience 26, 105800
January 20, 2023
https://doi.org/10.1016/j.isci.2022.105800

iScience

CellPress
OPEN ACCESS

Article

Comparative tissue proteomics reveals unique action mechanisms of vaccine adjuvants

Yibo Li,[1,2] Zhuofan Li,[1,2] and Xinyuan Chen[1,3,*]

SUMMARY

Radiofrequency adjuvant (RFA) was recently developed to boost influenza vaccination without the safety concerns of chemical adjuvants due to their physical nature. Yet, the action mechanisms of RFA remain largely unknown. Omics techniques offer new opportunities to identify molecular mechanisms of RFA. This study utilized comparative tissue proteomics to explore molecular mechanisms of the physical RFA. Comparison of RFA and chemical adjuvant (Alum, AddaVax, MPL, MPL/Alum)-induced tissue proteome changes identified 14 exclusively induced proteins by RFA, among which heat shock protein (HSP) 70 was selected for further analysis due to its known immune-modulating functions. RFA showed much weakened ability to boost ovalbumin and pandemic influenza vaccination in HSP70 knockout than wild-type mice, hinting crucial roles of HSP70 in RFA effects. This study supports comparative tissue proteomics to be an effective tool to study molecular mechanisms of vaccine adjuvants.

INTRODUCTION

Adjuvants play critical roles in developing new and improved vaccines.[1] Adjuvant discovery has been a slow process and mainly relied on empirical experience.[1–3] The most widely used Alum adjuvant was initially identified when Glenny and colleagues used aluminum salts to purify and concentrate diphtheria toxin and made an inadvertent finding that diphtheria toxin prepared by aluminum salt precipitation elicited higher titers of antibodies in guinea pigs.[4] The development of MF59 adjuvant was motivated to maintain the high potency while reducing the toxicity of Complete Freund's Adjuvant (CFA).[5] CFA is a water-in-oil emulsion adjuvant prepared by emulsifying killed Mycobacterium Tuberculosis in non-metabolizable mineral oil (paraffin oil and mannide monooleate).[5] MF59 uses squalene oil, an intermediate in the synthesis of cholesterol in human bodies, rather than non-metabolizing mineral oil, to prepare an oil-in-water emulsion, which significantly reduces local reactogenicity for safe use in humans.[5] Besides the widely used Alum and MF59 adjuvants, several Adjuvant System (AS)-based adjuvants have been also approved for human use that include AS01 and AS04.[6] AS-based adjuvants are combinations of classical adjuvants, immunostimulatory molecules, and formulations (e.g., emulsions, liposomes) to achieve an optimal activation of innate and adaptive immune systems.[6]

Due to the slow progress in developing classical adjuvants, we took a different approach to develop physical radiofrequency adjuvant (RFA).[7] Physical adjuvants intend to stimulate tissue stress and endogenous danger signal release to potentiate vaccine-induced immune responses. The development of physical adjuvants was inspired by recent progress in the elucidation of the mechanisms of widely used Alum and MF59 adjuvants, which lack specific cellular receptors to mediate their adjuvant effects. Studies found both adjuvants induced tissue stress and release of endogenous danger signals, such as uric acid, double-strand DNA (dsDNA), and ATP, to at least partially mediate their adjuvant effects.[8–11] Uric acid, dsDNA, and ATP belong to endogenous danger signals,[12,13] which are sequestered from immune cell recognition under physiological conditions and can release under tissue stress to alert the innate immune system of "danger". Physical adjuvants take advantage of well-controlled physical energies (e.g., laser, radiofrequency, and ultrasound) to induce tissue stress with the potential release of endogenous danger signals to enhance vaccine-induced immune responses. Physical adjuvants are also less likely to induce systemic adverse reactions due to their localized effects. We and several other groups explored the adjuvant effects of different types of laser to enhance intradermal (ID) vaccine-induced immune responses.[14–16] Considering different physical modalities might induce different tissue stress, we recently explored potential adjuvant effects of fractional bipolar RF treatment to boost ID vaccination.[7]

[1]Biomedical and Pharmaceutical Sciences, College of Pharmacy, University of Rhode Island, 7 Greenhouse Road, Avedisian Hall, Room 480, Kingston, RI 02881, USA

[2]These authors contributed equally

[3]Lead contact

*Correspondence: xchen14@uri.edu

https://doi.org/10.1016/j.isci.2022.105800

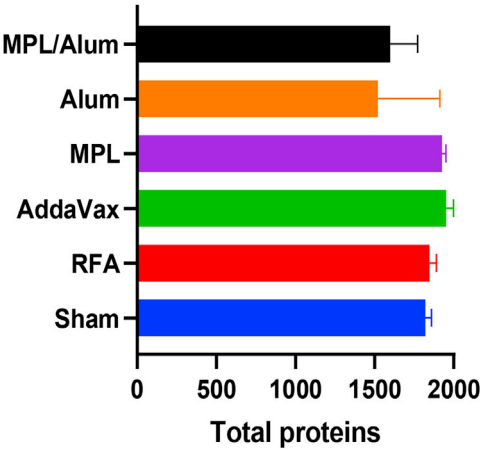

Figure 1. Total number of proteins

The lateral dorsal skin of mice was subjected to RFA or Sham treatment or intradermally injected with AddaVax, MPL, Alum, MPL/Alum. Skin was collected 18 h later and processed for SWATH-MS analysis. The total number of proteins detected was shown for each group (n = 3). Data were expressed as mean ± SEM.

We found physical RFA could significantly enhance ID ovalbumin (OVA) and recombinant hemagglutinin antigen (rHA)-induced humoral and cellular immune responses.[7] RFA showed comparable potency to MF59-mimetic AddaVax adjuvant to boost influenza pandemic 2009 H1N1 (pdm09) vaccination.[7] RFA induced transient, low-level local inflammation (e.g., cytokine and chemokine gene expression and immune cell recruitment), while chemical adjuvants, such as Alum, AddaVax, and MPL, elicited persistent and intense local inflammation.[7] RFA induced minimal systemic adverse reactions. RFA was found to significantly enhance influenza nucleoprotein (NP)-induced cellular immune responses and protection against lethal viral challenges.[17] RFA also showed potent adjuvant effects to enhance the low immunogenic H5N1 vaccination.[18]

Understanding the adjuvantation mechanisms is crucial for further development of the physical RFA for human use. Cutting-edge omics tools provide new opportunities to study vaccine adjuvant mechanisms. In fact, various omics tools (e.g., transcriptomics, proteomics, and metabolomics) have been successfully used in systems vaccinology to identify early or baseline immune signatures to predict vaccine-induced immune responses or reveal the unexpected link between microbiota and influenza vaccine responses in humans.[19,20] Transcriptomics has been used to study vaccine adjuvant-induced gene expression changes following intramuscular delivery in murine models.[21,22] One study found MF59 induced the most gene expression when compared to Alum and CpG adjuvants and all adjuvants induced 168 common gene expression.[23] Despite these interesting findings, the application of various omics techniques to study vaccine adjuvant mechanisms is still in its infancy.

This study utilized sequential windowed acquisition of all theoretical fragment ion mass spectra (SWATH-MS) proteomics to explore RFA-induced tissue proteome changes to identify novel signatures crucial for RFA effects.[24] SWATH-MS combines data-independent acquisition and targeted data analysis to achieve high accuracy, sensitivity, and selectivity for quantitative proteomics analysis in large scales.[25] Considering RFA likely works differently from chemical adjuvants, chemical adjuvant-induced tissue proteome changes were compared with RFA-induced tissue proteome changes. The comparative tissue proteomics allowed the identification of proteins exclusively stimulated by RFA, which were more likely to mediate RFA effects. Among these proteins, we specifically evaluated the potential roles of heat shock protein (HSP) 70 in RFA effects due to its immune-potentiating functions.[26] Using HSP70 knockout (KO) mice, we found HSP70 played a key role in RFA effects to boost ID OVA and pdm09 vaccination in murine models. Our study validated comparative tissue proteomics as an effective tool to study the action mechanisms of vaccine adjuvants.

RESULTS

Total number of proteins

We first compared the total proteins successfully detected in each group. One sample in the Sham group had significantly fewer proteins detected than other samples in the same group (1243 vs. 1825, 1778, 1857) and thus were excluded from the analysis. Overall, a total of 1820, 1847, 1953, 1926, 1521, and 1599 proteins were detected in Sham, RFA, AddaVax, MPL, Alum, and MPL/Alum groups, respectively (Figure 1). A similar

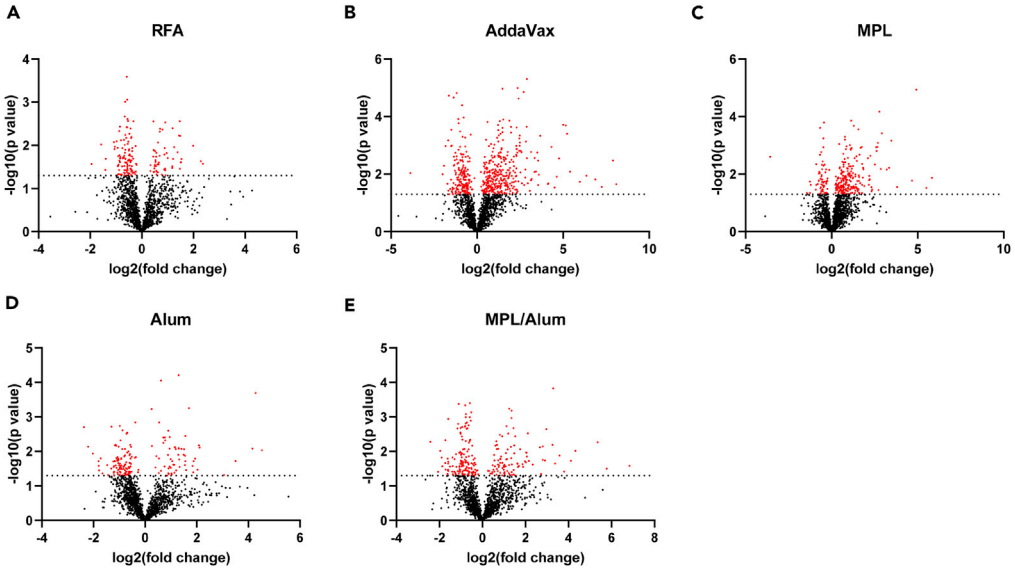

Figure 2. Volcano plots of DEPs

Volcano plots of DEPs induced by RFA, AddaVax, MPL, Alum, and MPL/Alum treatment were shown in (A–E), respectively. The x axis represented the log2(fold change) of the protein intensity after adjuvant treatment, while the y axis represented the statistical significance –log10(p value). One dot represented one protein and dots above the dashed line represented proteins with p value less than 0.05.

number of proteins detected in RFA and Sham groups (<1.5% difference) hinted the least impact of RFA on local tissue proteome. At least 5.8% more proteins were detected in AddaVax and MPL groups, indicating the significant induction of protein expression by these adjuvants. In contrast, at least 12% fewer proteins were detected in Alum and MPL/Alum groups. This might be the result of Alum-induced cell deaths rather than the mere inhibition of protein expression.[27] The significant reduction of protein expression in the MPL/Alum group hinted the dominant effect of Alum considering MPL-induced protein expression.

Differentially expressed proteins (DEPs)

Volcano plots were used to reveal DEPs after adjuvant treatment. As shown in Figure 2, AddaVax adjuvant induced the most protein expression followed by MPL adjuvant, while Alum and RFA induced the least protein expression. AddaVax also suppressed the most protein expression, while MPL suppressed the least protein expression (Figure 2). Similar results were obtained when the analysis was limited to DEPs with at least 30% expression changes (Table 1). Interestingly, 25.2% DEPs showed significantly changed levels in AddaVax group and 10.5-13.5% DEPs showed significantly changed levels in MPL, Alum, and MPL/Alum groups, while only 6.6% DEPs showed significantly changed levels in RFA group (Table 1). The above results hinted the physical RFA had the least impact on local tissue proteome, while AddaVax adjuvant had the most impact on local tissue proteome.

Table 1. DEPs with at least a 30% change in expression levels

	Increased		Reduced		Total	
	Number	Percentage	Number	Percentage	Number	Percentage
RFA	52	2.8%	70	3.8%	122	6.6%
Alum	60	3.9%	103	6.8%	163	10.7%
MPL/Alum	96	6.0%	118	7.4%	214	13.4%
MPL	204	10.6%	36	1.9%	240	12.5%
AddaVax	323	16.5%	170	8.7%	493	25.2%

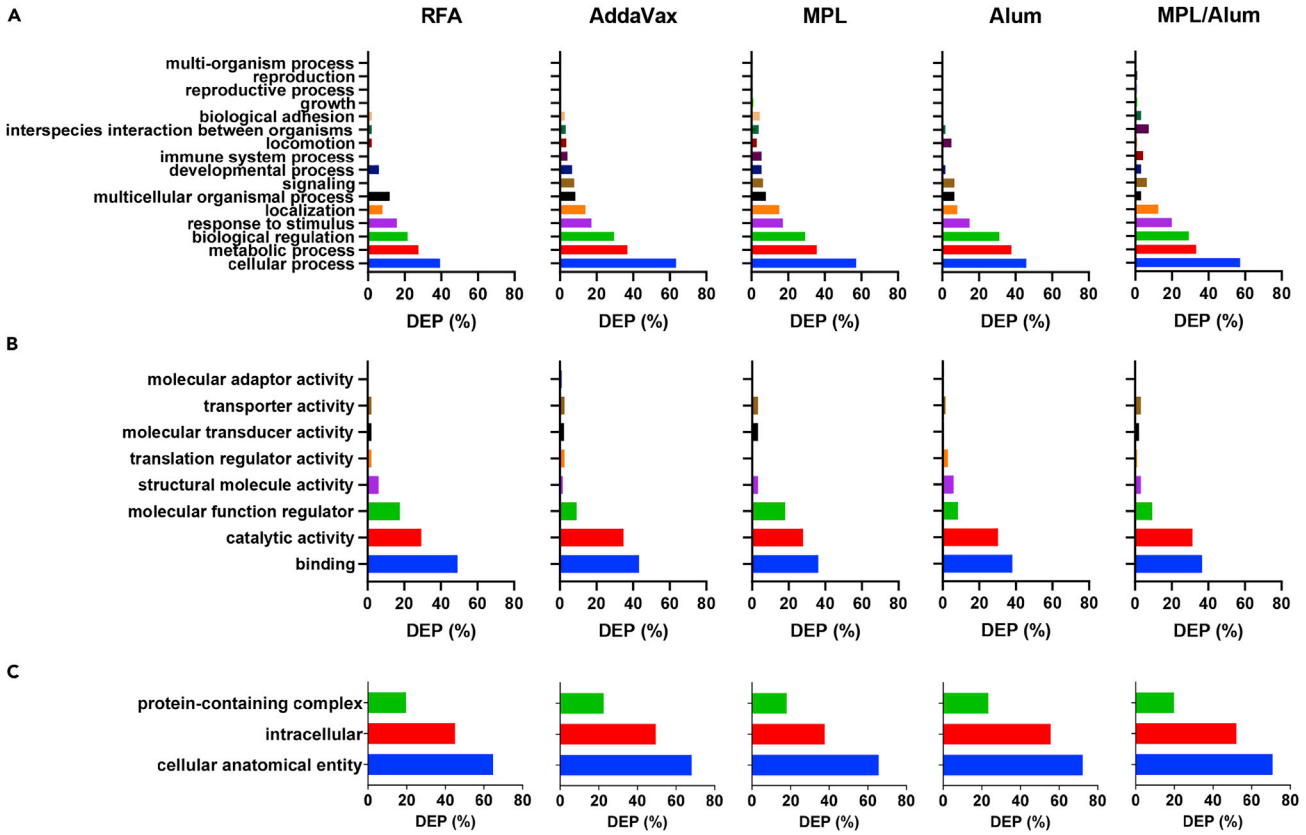

Figure 3. Gene Ontology functional analysis of DEPs

DEPs (induced) were subjected to Gene Ontology functional analysis via Panther Classification System (http://pantherdb.org). Analysis related to biological process, molecular function, and cellular component was shown in (A, B, and C), respectively. X axis reflected the percentage of DEPs.

Functional enrichment analysis

DEPs in Table 1 were subjected to Gene Ontology biological process, molecular function, and cellular component analysis. The majority of the DEPs can be classified into four major biological processes with descending orders regardless of the adjuvant types: cellular process, metabolic process, biological regulation, and response to stimuli (Figure 3A). Interestingly, RFA induced a smaller percentage of DEPs in the cellular process (39.2% vs. 45.9-63.4%), metabolic process (27.5% vs. 35.6-37.7%), and biological regulation (21.6% vs. 29.2-31.1%) when compared to chemical adjuvants (Figure 3A). Yet, RFA induced a similar percentage of DEPs in response to stimuli to chemical adjuvants (15.7% vs. 14.8-19.8%, Figure 3A). To be noted, combinatorial MPL/Alum adjuvant induced a higher percentage of DEPs in response to stimuli (19.8% vs. 17.1% and 14.8%), while a similar percentage of DEPs in other major categories, when compared to MPL or Alum adjuvant (Figure 3A). As for molecular function, the majority of DEPs could be classified into binding, catalytic activity, and molecular function regulator categories with descending orders regardless of adjuvant types (Figure 3B). Interestingly, the physical RFA induced the highest percentage of DEPs in the binding and molecular function categories combined (Figure 3B). As for the cellular component, physical and chemical adjuvants elicited similar percentages of DEPs in all three categories (Figure 3C).

Shared differentially expressed proteins among adjuvants

Different adjuvants likely activate different signaling pathways, stimulate different cytokine and chemokine expressions, recruit different types of innate immune cells, resulting in different tissue proteome changes. Next, a web-based tool (InteractiVenn) was used to explore similarities of adjuvant-induced DEPs in Table 1.[28] Interestingly, we found all adjuvants (physical and chemical) stimulated two common protein expression (encoded by *Itih2* and *Serpinf2*) (Figure 4A). *Itih2* encodes inter-alpha-trypsin inhibitor heavy chain H2. The inter-alpha-trypsin inhibitors are a family of plasma protease inhibitors, assembled from a

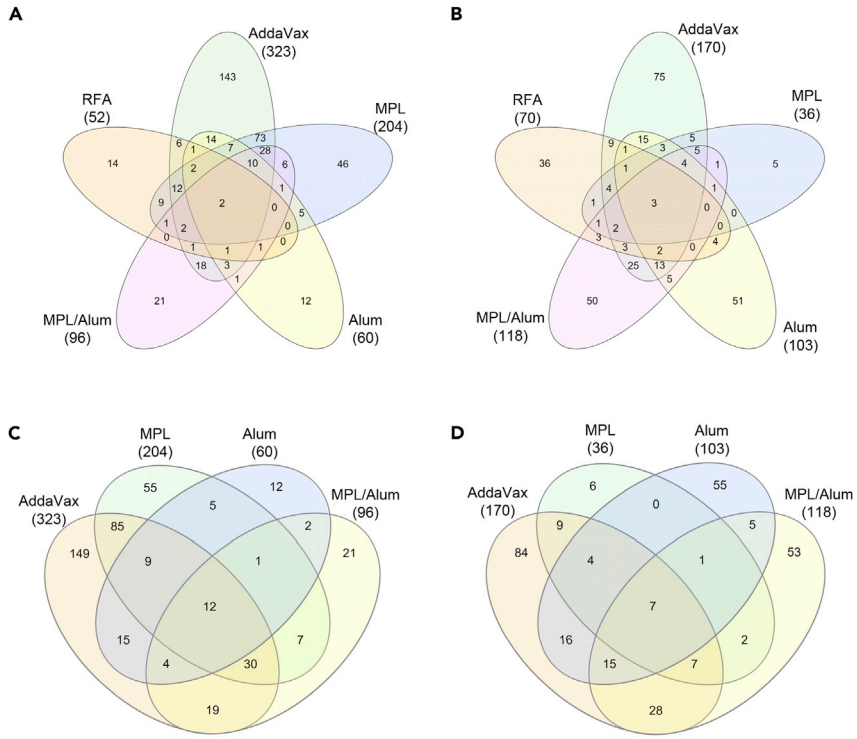

Figure 4. Shared DEPs among adjuvants

DEPs were subjected to InteractiVenn analysis (http://www.interactivenn.net/).

(A) Venn diagram about adjuvant-induced DEPs.

(B) Venn diagram about adjuvant-suppressed DEPs.

(C) Venn diagram of chemical adjuvant-induced DEPs.

(D) Venn diagram of chemical adjuvant-suppressed DEPs. Number in the parentheses indicated the total number of DEPs.

light chain (bikunin) and five homologous heavy chains (encoded by *Itih1, Itih2, Itih3, Itih4,* and *Itih5*), contributing to extracellular matrix stability by covalent linkage to hyaluronan. *Serpinf2* encodes alpha-2-antiplasmin, which is a serine protease inhibitor responsible for inactivating plasmin. All adjuvants (physical and chemical) suppressed three common protein expressions (encoded by *Acta1, Palld, and Pdxk*) (Figure 4B). *Acta1* encodes actin alpha 1, which is one of the six actin isoforms identified. Actins are highly conserved proteins that are involved in cell motility, structure, and integrity. Alpha actins are a major constituent of the contractile apparatus. *Palld* encodes Palladin, which is a component of actin-containing microfilaments that control cell shape, adhesion, and contraction. *Pdxk* encodes pyridoxal kinase, which is a cytoplasmic protein that phosphorylates vitamin B6. The modulation of common protein expression indicated some similarities of the different adjuvants.

Due to the big difference between physical and chemical adjuvants, we further analyzed common proteins regulated by chemical adjuvants. As shown in Figure 4C, there were 12 DEPs induced by all chemical adjuvants (encoded by *Chil3, Camp, Lcn2, Itih2, Cyc1, H2-Q10, Mapk14, Serpinf2, Rps15a, Rab2a, Vdac3, and Psat1*). Among the 12 proteins, at least 5 proteins have important roles in inflammation and immunity (encoded by *Chil3, Camp, Lcn2, H2-Q10, and Mapk14*). *Chil3* encodes chitinase-like protein 3 with important roles in regulating functions of eosinophils, macrophages, neutrophils, T and B cells.[29,30] *Camp* encodes cathelicidin antimicrobial peptide, which is primarily stored in the lysosomes of macrophages and polymorphonuclear leukocytes (PMNs) and has antimicrobial functions.[31] *Lcn2* encodes lipocalin 2, which is a neutrophil gelatinase-associated lipocalin (NGAL) and can be released by various cell types and is an attractive marker of inflammation and infection.[32] *H2-Q10* encodes H-2 class I histocompatibility antigen Q10 alpha chain that is involved in the presentation of foreign antigens to the immune system (325 aa). *Mapk14* encodes one of the four p38 mitogen-activated protein kinases (MAPKs) with important roles in the cascades of cellular responses evoked by extracellular stimuli, such as proinflammatory cytokines or physical stress, leading to the direct activation of transcriptional factors.[33] Among other proteins, six of

Table 2. List of genes encoding uniquely induced proteins by vaccine adjuvants

RFA	AddaVax		Alum	MPL	MPL/Alum
Ddx6	*Aars*	*Kpnb1*	*Ahsg*	*Acbd3*	*1700074P13Rik*
Efhd2	*Acot7*	*Krt84*	*C4b*	*Anxa4*	*Arf4*
Flg2	*Actb*	*Lasp1*	*C8a*	*Anxa7*	*Cox4i1*
Hspa1b	*Actbl2*	*Lifr*	*C8g*	*Anxa8*	*Eif3m*
Lrrfip2	*Actn1*	*Lmnb1*	*Irf2bpl*	*Apcs*	*Gpld1*
Nfu1	*Add1*	*Ly6c2*	*Klhl40*	*Bag1*	*Gstm2*
Nucb2	*Adprh*	*Man2b1*	*Krt33a*	*Ccar1*	*Gusb*
Pbdc1	*Agt*	*Marcks*	*Mif*	*Cd47*	*Hbb-bs*
Rcn1	*Ahcy*	*Mbl2*	*Serpina3k*	*Cdc5l*	*Ig heavy chain V region 6.96*
Set	*Anp32a*	*Mcm3*	*Sfxn3*	*Copb2*	*Igkv13-84*
Srsf1	*Anxa11*	*Mcm7*	*Stfa3*	*Crip2*	*Klc3*
Tnxb	*Anxa3*	*Mmp8*	*Timm13*	*Ctsz*	*Ly6a*
Txn2	*Apbb1ip*	*Mpo*		*Dnajb11*	*Mapk1*
Vcan	*Apoc1*	*Msra*		*Dsg1b*	*Nars*
	Atic	*Mug1*		*Eif2s2*	*Ndufb11*
	Atp1a1	*Nampt*		*Eif5*	*Rac1*
	Atp6v0d1	*Ncf4*		*Fga*	*Rars*
	Atp6v1e1	*Neb*		*Fgb*	*Rpsa*
	Azgp1	*Nfkb1*		*Fgg*	*Slc25a3*
	Bzw1	*Ostf1*		*G3bp1*	*Tmed10*
	Cand1	*Pa2g4*		*Hist1h1c*	*Tmprss13*
	Canx	*Padi4*		*Hp*	
	Caprin1	*Pak2*		*Hspa5*	
	Cct3	*Pcna*		*Ifi205a*	
	Cct6a	*Pdcd6ip*		*Ifi35*	
	Cct8	*Pfas*		*Lamp2*	
	Cd9	*Phb2*		*Lrg1*	
	Celf2	*Pkm*		*Metap2*	
	Ces1c	*Plg*		*Mpp1*	
	Cfi	*Pnkp*		*Mvp*	
	Ckap4	*Prdx5*		*Naca*	
	Cltc	*Prep*		*Npc2*	
	Cnn2	*Prpf19*		*Nudc*	
	Copg1	*Prtn3*		*Orm1*	
	Coro7	*Psma2*		*Pacsin2*	
	Cotl1	*Psma4*		*Pnp*	
	Cpne3	*Psmb1*		*Ppid*	
	Cwc15	*Psmd13*		*Psmd1*	
	Cyfip2;Cyfip1	*Qsox1*		*Rpl14*	
	Dars	*Rala;Ralb*		*Rpl27a*	
	Dcps	*Ran*		*Sar1b*	
	Ddost	*Rbbp4*		*St13*	
	Ddx39b	*Rhoa*		*Stfa1*	
	Dync1li1	*Rnpep*		*Twf1*	
	Dync1li2	*Rpia*		*Urah*	

(*Continued on next page*)

Table 2. *Continued*

RFA	AddaVax		Alum	MPL	MPL/Alum
	Dynll1	*Septin-6*		*Wars*	
	Eef1a1	*Sf3a3*			
	Eif2s3x	*Slc25a12*			
	Eif3a	*Slc9a3r1*			
	Eif3b	*Snrpa*			
	Ezr	*Srrt*			
	F10	*Srsf2*			
	F13b	*Ssb*			
	Fbln1	*Sun2*			
	Fetub	*Syncrip*			
	Fis1	*Taldo1*			
	Gart	*Tcn2*			
	Gda	*Tcp1*			
	Gnai2	*Tf*			
	Gpd2	*Tkt*			
	Gpi	*Tln1*			
	Gpx3	*Tmed9*			
	Gpx4	*Tpm3-rs7*			
	Grb2	*Trim28*			
	H2afy	*Twf2*			
	Hck	*Ube2d3;Ube2d1;Ube2d2*			
	Hmgb2	*Vasp*			
	Hsd17b10	*Vcl*			
	Hsp90aa1	*Vps35*			
	Il1rap	*Wdr1*			
	Impa2	*Zyx*			
	Impdh2				

Note: alphabetic order.

them have important roles in metabolism according to pathway analysis by Reactome (encoded by *Itih2, Cyc1, Rps15a, Rab2a, Vdac3, and Psat1*). Besides the previously introduced *Itih2, Cyc1* encodes the respiratory subunit of ubiquinol cytochrome *c* reductase (complex III), which is located in the inner mitochondrial membrane and is part of the electron transport chain. *Rps15a* encodes a ribosomal protein that is a component of the 40S subunit. *Rab2a* encodes a small GTPase with important roles in vesicular fusion and trafficking. *Vdac3* encodes the mammalian voltage-dependent anion-selective channel protein 3 of the outer mitochondrial membrane with a role in reactive oxygen species homeostasis.[34] *Psat1* encodes phosphoserine aminotransferase 1 with a role in serine biosynthesis.

Chemical adjuvants suppressed 7 common protein expressions (encoded by *Acta1, Dpt, Peg3, Palld, Pdxk, Krt13, and Selenbp1*). Besides previously introduced *Acta1, Palld, and Pdxk*, *Dpt* encodes dermatopontin, a component of the extracellular matrix, with potential functions in cell-matrix interactions and matrix assembly. *Peg3* encodes paternally expressed gene 3 protein with a potential role in cell proliferation and p53-mediated apoptosis. *Krt13* encodes keratin 13, which is a type I cytokeratin paired with keratin 4 and expressed in the suprabasal layers of non-cornified, stratified epithelia. *Selenbp1* encodes selenium binding protein 1 with important roles in protein degradation, cell differentiation, and motility.[35]

Exclusively induced proteins reveal action mechanisms of radiofrequency adjuvant

While shared DEPs reflected similarities of adjuvants, exclusively induced proteins might indicate the unique action mechanisms of adjuvants. A simple calculation found AddaVax adjuvant stimulated 44%

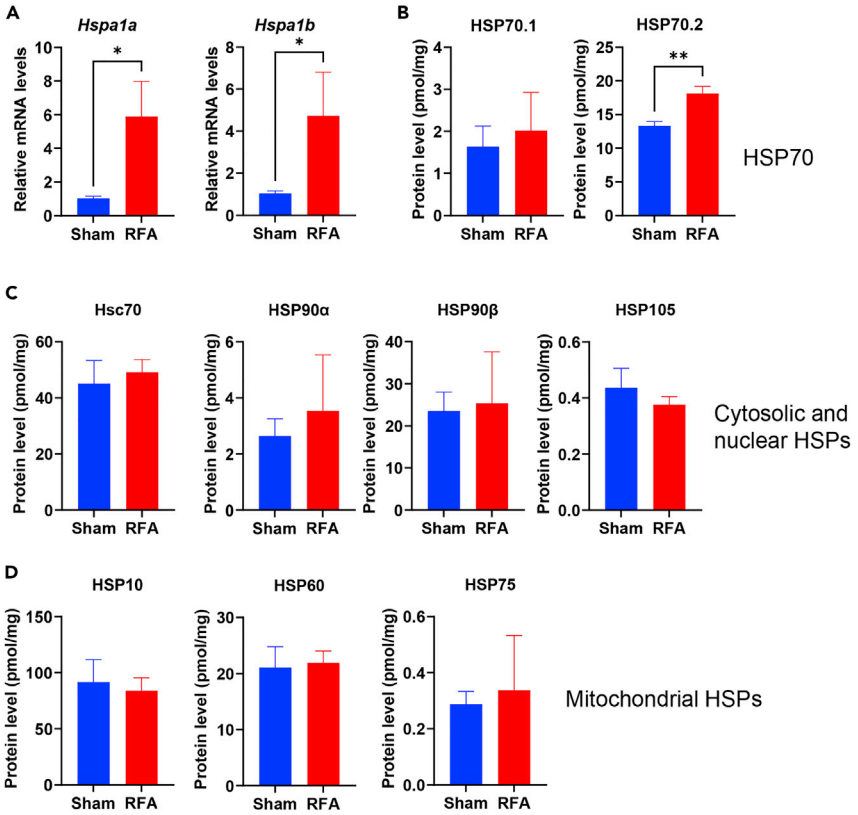

Figure 5. RFA only increases HSP70 levels

(A) Relative mRNA levels at 6 h after RFA or Sham treatment. n = 5 in Sham and n = 4 in RFA.

(B) Protein levels of HSP70.1 and HSP70.2 obtained from proteomics study.

(C) Protein levels of Hsc70, HSP90α, HSP90β, and HSP105 obtained from proteomics study.

(D) Protein levels of mitochondrial HSP10, HSP60, and HSP75 obtained from proteomics study. n = 3 in (B–D). Two-tailed Student's *t* test was used to compare differences between groups. *, $p<0.05$; **, $p < 0.01$. Data were expressed as mean ± SEM.

of uniquely expressed proteins, RFA stimulated 27% of uniquely expressed proteins, and the remaining adjuvants stimulated 20-23% of uniquely expressed proteins. The genes encoding the uniquely induced proteins by vaccine adjuvants were listed in Table 2. Next, we focused on exploring exclusively induced proteins and their potential roles in RFA effects.

There were 14 uniquely expressed proteins induced by RFA (encoded by *Nfu1, Lrrfip2, Rcn1, Set, Vcan, Tnxb, Ddx6, Pbdc1, Txn2, Efhd2, Nucb2, Srsf1, Hspa1b, Flg2*). Among these, *Hspa1b* attracted our attention since this gene encoded HSP70.2, which was found to be induced by RFA in our prior western blotting analysis.[7] Considering HSP70 expression was initiated by the transcription of closely linked *Hspa1a* and *Hspa1b* genes,[36] we evaluated their mRNA levels at an early time point (6 h). We found RFA significantly increased *Hspa1a* and *Hspa1b* mRNA levels when compared to Sham treatment (Figure 5A). We also analyzed protein levels of HSP70.1 encoded by *Hspa1a*, HSP70.2 encoded by *Hspa1b*, and other HSPs, such as constitutively expressed Hsc70, cytosolic and nuclear HSP90, and HSP105, and also mitochondrial HSP10, HSP60, and HSP75.[36] As shown in Figure 5B, RFA significantly increased HSP70.2 levels. HSP70.1 levels in the RFA group increased but didn't reach a statistically significant level. RFA didn't significantly change other HSP levels (Figures 5C and 5D), in line with our prior report.[7]

To explore a potential role of HSP70 in RFA effects, wild-type (WT) and HSP70 KO mice were prime/boost immunized with OVA in the presence of RFA or Sham followed by the measurement of serum anti-OVA antibody titer 3 weeks after prime and boost, as illustrated in Figure 6A. OVA immunization

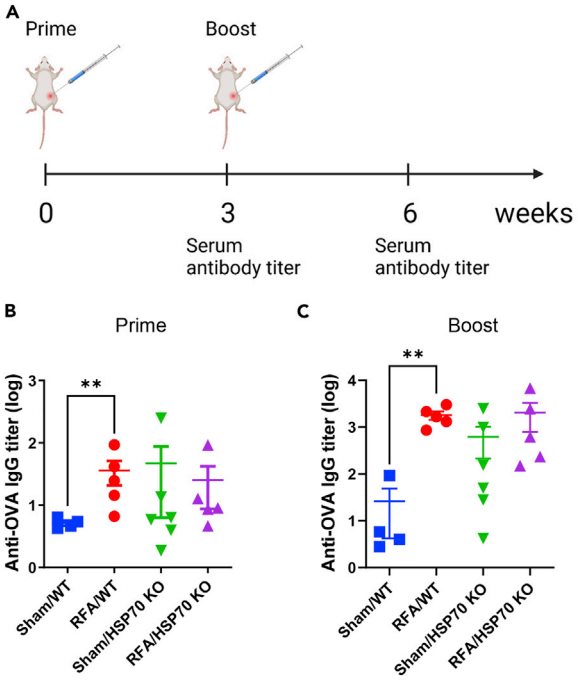

Figure 6. Key roles of HSP70 in RFA to boost ID OVA immunization

WT and HSP70 KO mice in the C57BL/6 background were subjected to RFA or Sham treatment followed by the ID injection of 10 μg OVA into RFA or Sham-treated skin. Immunization was repeated 3 weeks later. Serum anti-OVA antibody titer was measured 3 weeks after each immunization.

(A) Illustration of experimental schedule.

(B) Serum anti-OVA antibody titer after prime.

(C) Serum anti-OVA antibody titer after boost. n = 4-6. Student's *t* test was used to compare differences between RFA and Sham groups. **, $p < 0.01$. Data were expressed as mean ± SEM.

with prior RFA treatment induced significantly higher anti-OVA antibody titer than OVA immunization with prior Sham treatment in WT mice (Figures 6B and 6C). However, OVA immunization with prior RFA treatment failed to elicit significantly higher anti-OVA antibody titer than OVA immunization with prior Sham treatment in HSP70 KO mice (Figures 6B and 6C). This study indicated significantly weakened RFA effects in HSP70 KO mice, supporting the crucial roles of HSP70 in RFA effects to boost ID OVA immunization.

We further explored whether HSP70 played a crucial role in RFA to boost influenza vaccination. To this end, WT and HSP70 KO mice were subjected to RFA or Sham treatment followed by the ID injection of pdm09 vaccine into RFA or Sham-treated skin. As shown in Figures 7A and 7B, RFA significantly increased pdm09 vaccine-induced HI titer and anti-rHA IgG titer in WT but not HSP70 KO mice. Serum HI titer was also significantly higher in RFA/WT than RFA/HSP70 KO mice (Figure 7A). Following lethal viral challenges, pdm09 vaccination in the presence of RFA conferred significant protection against body weight loss in WT but not HSP70 KO mice (Figures 7C and 7D). Pdm09 vaccination in the presence of RFA also conferred significantly better protection against body weight loss in WT than in HSP70 KO mice (Figure S1). The majority of WT and HSP70 KO mice in NI or Sham groups either died or lost more than 25% body weight (humane endpoint) within 9 days (Figures 7C and 7D). In contrast, WT mice in the RFA group only lost a maximal 8% body weight on day 8 followed by a quick recovery to their original body weights on day 10 (Figure 7C). HSP70 KO mice in the RFA group lost a maximal 16% body weight on day 7 and didn't recover to their original body weights on day 14 (Figure 7D). RFA significantly increased the survival of WT but not HSP70 KO mice (Figures 7E and 7F). About 67% of WT mice in the RFA group survived, while all WT mice in NI and Sham groups died in 10 days (Figure 7E). In HSP70 KO mice, 30% of mice survived in the RFA group and 11% of mice survived in the Sham group and all mice died in the NI group (Figure 7F). The above data indicated HSP70 played a crucial role in RFA effects to boost pdm09 vaccination.

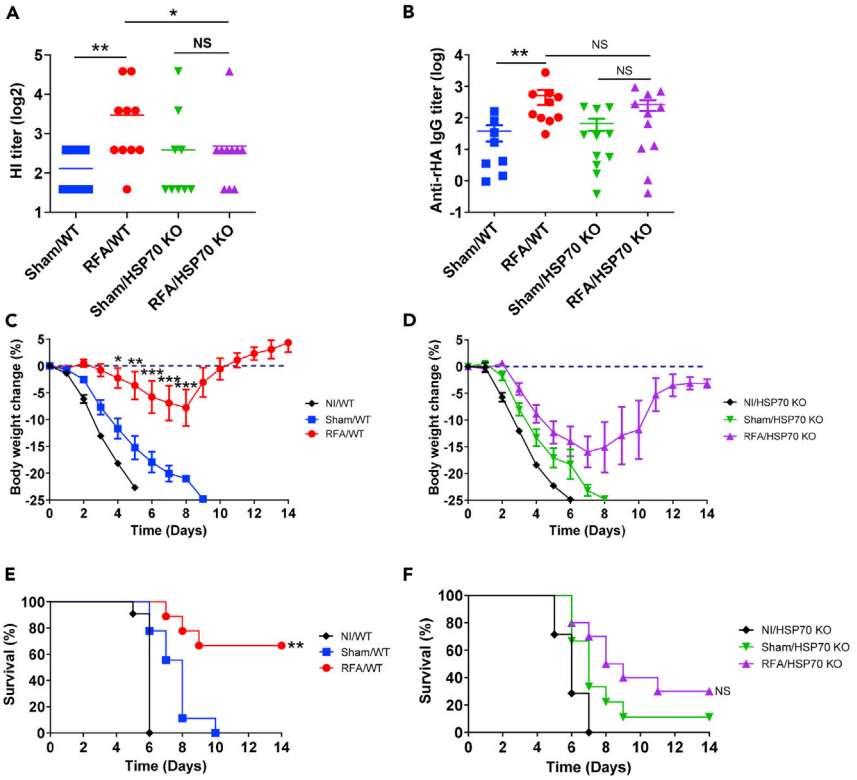

Figure 7. Crucial roles of HSP70 in RFA to boost ID pdm09 vaccination

(A and B) WT and HSP70 KO mice were subjected to RFA or Sham treatment followed by the ID injection of 0.3 μg pdm09 vaccine into RFA or Sham-treated skin or left non-immunized (NI). Serum HI (A) and anti-rHA antibody titers (B) were measured 3 weeks later.

(C–F) The above-immunized mice were intranasally challenged with 10× LD_{50} of mouse-adapted pdm09 viruses 4 weeks after immunization. Body weight change (C and D) and survival (E and F) were monitored daily for 14 days. Two-tailed Mann-Whitney U test was used to compare differences between RFA and Sham groups in (A and B). Two-way ANOVA with Bonferroni's multiple comparison test was used to compare differences in body weight change between RFA and Sham groups at different time points in (C and D). Log rank test with Bonferroni's correction was used to compare differences in survival between RFA and Sham groups in (E and F). *, $p < 0.05$; **, $p < 0.01$; ***, $p < 0.001$. NS: not significant. n = 9-11. Data were expressed as mean ± SEM. Experiments were repeated twice with similar results.

DISCUSSION

Adjuvant mechanism studies mainly focus on identifying cellular receptors and downstream signaling pathways and exploring cytokine and chemokine release profiles, immune cell recruitment kinetics, and antigen uptake, migration, and maturation of dendritic cells (DCs).[37–39] Gene-knockout mice and pharmacological inhibitors are used to study molecular mechanisms. These conventional tools lack the power to identify novel molecular signatures crucial for vaccine adjuvant effects. To our knowledge, this study remains one of the first to use comparative tissue proteomics to identify DEPs and study their potential roles in vaccine adjuvant effects. We focused on our recently developed RFA and successfully identified one of the uniquely induced proteins (HSP70) as a key player in RFA effects. Besides HSP70, RFA likely stimulated other mechanisms to mediate its adjuvant effects. In support, pdm09 vaccination with prior RFA treatment elicited better antibody responses and protection than pdm09 vaccination with prior Sham treatment in HSP70 KO mice despite the lack of significant differences between the two groups. Although HSP70 was identified as a key player in RFA effects, more mechanistic studies are required to elucidate how *in situ* generated HSP70 enhanced ID vaccine-induced immune responses. Due to the immune-potentiating effects of extracellular HSP70,[26] RFA-induced HSP70 may gain access to extracellular space to bind and transport ID antigens to DCs and may also stimulate DC maturation to enhance vaccine-induced immune responses.

This study also identified DEPs induced by commonly used chemical adjuvants, which can be further screened to study their roles in vaccine adjuvant effects. Despite the significant progress made in the last two decades, the action mechanisms of commonly used chemical adjuvants were only partially understood. For instance, Alum-induced dsDNA release was found to stimulate canonical T helper 2 (Th2) responses and IgE isotype switching via interferon regulatory factor (IRF) 3-dependent mechanisms.[8,40] Yet, the signaling pathways underlying dsDNA-induced IgG1 antibody responses were not clear.[8,40] MF59 was found to stimulate myeloid differentiation primary response 88 (MyD88) pathway to mediate its adjuvant effects.[41] Yet, how MyD88 was activated remained a mystery. Although MPL is known to activate TLR4 and MyD88 signaling pathway,[42] key molecules that mediate the increased antigen uptake and DC maturation remain largely unknown. The underlying mechanisms of the synergistic effects of MPL and Alum in the combinatorial AS04 adjuvant remain to be explored.

Our current study utilized gene-knockout mice to explore the underlying roles of HSP70 in RFA effects. Other methods can also be used to study the potential roles of target proteins in vaccine adjuvant effects that include *in vivo* siRNA, neutralizing antibodies, and pharmacological inhibitors. When studying the action mechanisms of chemical adjuvants, cell culture can also be used. In that case, DCs can be treated with chemical adjuvants in the presence of siRNA or inhibitors against the interested targets followed by the evaluation of cytokine/chemokine release or DC maturation. DC/T cell co-culture can also be used to further study T cell activation and differentiation. If knockout mice are available, DCs of WT and knockout mice can be compared in response to chemical adjuvant treatment. Overall, comparative tissue proteomics can be combined with conventional methods to study molecular mechanisms of vaccine adjuvants.

We also made interesting findings in this study. MF59-mimetic AddaVax adjuvant showed the most impact on local tissue proteome and all chemical adjuvants induced 12 common protein expressions. These findings were consistent with a prior transcriptomics study, which found MF59 induced the most gene expression and all chemical adjuvants induced a common set of 168 gene expression.[23] The least impact of RFA on local tissue proteome was also in line with our prior study, in which we found RFA induced transient, low-level local inflammation.[7]

Comparative tissue proteomics offers unique opportunities to identify exclusively induced proteins and study their roles in vaccine adjuvant effects. Yet, comparative tissue proteomics cannot capture non-protein-related mechanisms, such as those mediated by the release of preexisting endogenous danger signals (e.g., ATP, dsDNA, uric acid). Considering endogenous danger signals might activate specific signaling pathways and induce protein expression, comparative tissue proteomics can still be used to study vaccine adjuvant mechanisms in this regard. Besides traditional proteomics, recent emerging of phosphoproteomics offers another tool to study global phosphorylation changes and adjuvant-induced signaling pathways.[43]

Limitations of the study

Our current study had 3 samples per group. The small sample size only allowed proteins with less variable levels to be identified. An increase in sample size is expected to allow more DEPs to be detected. Besides this limitation, our current study failed to detect the majority of cytokines and chemokines. Although this is expected in the consideration of their extremely low levels and the diluted tissue environment,[44] comparative tissue proteomics will benefit from prior fractionation and enrichment steps to increase the detection sensitivity for cytokines and chemokines, which are relevant to vaccine adjuvant effects.

STAR★METHODS

Detailed methods are provided in the online version of this paper and include the following:

- KEY RESOURCES TABLE
- RESOURCE AVAILABILITY
  - Lead contact
  - Materials availability
  - Data and code availability
- EXPERIMENTAL MODEL AND SUBJECT DETAILS
  - Mice
- METHOD DETAILS

- RFA treatment
- Chemical adjuvant treatment
- Immunization
- HI titer
- ELISA antibody titer
- Lethal viral challenge
- Real-time PCR
- Skin processing for proteomics analysis
- LC-MS/MS
- Data processing
- Data analysis
- Bioinformatics analysis

- QUANTIFICATION AND STATISTICAL ANALYSIS

SUPPLEMENTAL INFORMATION

Supplemental information can be found online at https://doi.org/10.1016/j.isci.2022.105800.

ACKNOWLEDGMENTS

This work is supported by the National Institutes of Health grant AI139473 (to X.Y.C.). Microplate reader used in this work is supported by the Rhode Island Institutional Development Award (IDeA) Network of Biomedical Research Excellence from the National Institute of General Medical Sciences of the National Institutes of Health grant P20GM103430. We would like to thank Nicholas DaSilva for helping with LC-MS/MS sample running and Spectronaut data analysis. We would also like to thank Christopher Hemme for assistance with proteomics data analysis.

AUTHOR CONTRIBUTIONS

X.Y.C. designed experiments; Y.B.L. and Z.F.L. conducted experiments and acquired data; X.Y.C., Y.B.L., and Z.F.L. analyzed data; X.Y.C. and Y.B.L. wrote the article.

DECLARATION OF INTERESTS

The authors declare no competing interests.

INCLUSION AND DIVERSITY

We support inclusive, diverse, and equitable conduct of research.

Received: September 16, 2022
Revised: November 10, 2022
Accepted: December 8, 2022
Published: January 20, 2023

REFERENCES

1. Reed, S.G., Orr, M.T., and Fox, C.B. (2013). Key roles of adjuvants in modern vaccines. Nat. Med. *19*, 1597–1608. https://doi.org/10.1038/nm.3409.

2. Di Pasquale, A., Preiss, S., Tavares Da Silva, F., and Garçon, N. (2015). Vaccine adjuvants: from 1920 to 2015 and beyond. Vaccines *3*, 320–343. https://doi.org/10.3390/vaccines3020320.

3. McKee, A.S., and Marrack, P. (2017). Old and new adjuvants. Curr. Opin. Immunol. *47*, 44–51. https://doi.org/10.1016/j.coi.2017.06.005.

4. Marrack, P., McKee, A.S., and Munks, M.W. (2009). Towards an understanding of the adjuvant action of aluminium. Nat. Rev. Immunol. *9*, 287–293. https://doi.org/10.1038/nri2510.

5. O'Hagan, D.T., Ott, G.S., Nest, G.V., Rappuoli, R., and Giudice, G.D. (2013). The history of MF59((R)) adjuvant: a phoenix that arose from the ashes. Expert Rev. Vaccines *12*, 13–30. https://doi.org/10.1586/erv.12.140.

6. Garçon, N., Chomez, P., and Van Mechelen, M. (2007). GlaxoSmithKline adjuvant systems in vaccines: concepts, achievements and perspectives. Expert Rev. Vaccines *6*, 723–739. https://doi.org/10.1586/14760584.6.5.723.

7. Cao, Y., Zhu, X., Hossen, M.N., Kakar, P., Zhao, Y., and Chen, X. (2018). Augmentation of vaccine-induced humoral and cellular immunity by a physical radiofrequency adjuvant. Nat. Commun. *9*, 3695. https://doi.org/10.1038/s41467-018-06151-y.

8. Marichal, T., Ohata, K., Bedoret, D., Mesnil, C., Sabatel, C., Kobiyama, K., Lekeux, P., Coban, C., Akira, S., Ishii, K.J., et al. (2011). DNA released from dying host cells mediates aluminum adjuvant activity. Nat. Med. *17*, 996–1002. https://doi.org/10.1038/nm.2403.

9. McKee, A.S., Burchill, M.A., Munks, M.W., Jin, L., Kappler, J.W., Friedman, R.S., Jacobelli, J., and Marrack, P. (2013). Host DNA released in response to aluminum adjuvant enhances MHC class II-mediated antigen presentation and prolongs CD4 T-cell interactions with dendritic cells. Proc. Natl. Acad. Sci. USA *110*,

E1122–E1131. https://doi.org/10.1073/pnas.1300392110.

10. Kool, M., Soullié, T., van Nimwegen, M., Willart, M.A.M., Muskens, F., Jung, S., Hoogsteden, H.C., Hammad, H., and Lambrecht, B.N. (2008). Alum adjuvant boosts adaptive immunity by inducing uric acid and activating inflammatory dendritic cells. J. Exp. Med. *205*, 869–882. https://doi.org/10.1084/jem.20071087.

11. Vono, M., Taccone, M., Caccin, P., Gallotta, M., Donvito, G., Falzoni, S., Palmieri, E., Pallaoro, M., Rappuoli, R., Di Virgilio, F., et al. (2013). The adjuvant MF59 induces ATP release from muscle that potentiates response to vaccination. Proc. Natl. Acad. Sci. USA *110*, 21095–21100. https://doi.org/10.1073/pnas.1319784110.

12. Schaefer, L. (2014). Complexity of danger: the diverse nature of damage-associated molecular patterns. J. Biol. Chem. *289*, 35237–35245. https://doi.org/10.1074/jbc.R114.619304.

13. Kono, H., and Rock, K.L. (2008). How dying cells alert the immune system to danger. Nat. Rev. Immunol. *8*, 279–289. https://doi.org/10.1038/nri2215.

14. Chen, X., Wang, J., Shah, D., and Wu, M.X. (2013). An update on the use of laser technology in skin vaccination. Expert Rev. Vaccines *12*, 1313–1323. https://doi.org/10.1586/14760584.2013.844070.

15. Chen, X., and Wu, M.X. (2011). Laser vaccine adjuvant for cutaneous immunization. Expert Rev. Vaccines *10*, 1397–1403. https://doi.org/10.1586/erv.11.112.

16. Kashiwagi, S., Brauns, T., Gelfand, J., and Poznansky, M.C. (2014). Laser vaccine adjuvants. History, progress, and potential. Hum. Vaccin. Immunother. *10*, 1892–1907. https://doi.org/10.4161/hv.28840.

17. Li, Y., Li, Z., Zhao, Y., and Chen, X. (2021). Potentiation of recombinant NP and M1-induced cellular immune responses and protection by physical radiofrequency adjuvant. Vaccines *9*. https://doi.org/10.3390/vaccines9121382.

18. Li, Z., Kim, K.H., Bhatnagar, N., Park, B.R., Jeeva, S., Jung, Y.J., Raha, J., Kang, S.M., and Chen, X. (2022). Physical radiofrequency adjuvant enhances immune responses to influenza H5N1 vaccination. FASEB J. *36*, e22182. https://doi.org/10.1096/fj.202101703R.

19. Shannon, C.P., Blimkie, T.M., Ben-Othman, R., Gladish, N., Amenyogbe, N., Drissler, S., Edgar, R.D., Chan, Q., Krajden, M., Foster, L.J., et al. (2020). Multi-omic data integration allows baseline immune signatures to predict hepatitis B vaccine response in a small cohort. Front. Immunol. *11*, 578801. https://doi.org/10.3389/fimmu.2020.578801.

20. Pulendran, B., S Arunachalam, P., and O'Hagan, D.T. (2021). Emerging concepts in the science of vaccine adjuvants. Nat. Rev. Drug Discov. *20*, 454–475. https://doi.org/10.1038/s41573-021-00163-y.

21. Olafsdottir, T., Lindqvist, M., and Harandi, A.M. (2015). Molecular signatures of vaccine adjuvants. Vaccine *33*, 5302–5307. https://doi.org/10.1016/j.vaccine.2015.04.099.

22. O'Connor, D., and Pollard, A.J. (2013). Characterizing vaccine responses using host genomic and transcriptomic analysis. Clin. Infect. Dis. *57*, 860–869. https://doi.org/10.1093/cid/cit373.

23. Mosca, F., Tritto, E., Muzzi, A., Monaci, E., Bagnoli, F., Iavarone, C., O'Hagan, D., Rappuoli, R., and De Gregorio, E. (2008). Molecular and cellular signatures of human vaccine adjuvants. Proc. Natl. Acad. Sci. USA *105*, 10501–10506. https://doi.org/10.1073/pnas.0804699105.

24. Ludwig, C., Gillet, L., Rosenberger, G., Amon, S., Collins, B.C., and Aebersold, R. (2018). Data-independent acquisition-based SWATH-MS for quantitative proteomics: a tutorial. Mol. Syst. Biol. *14*, e8126. https://doi.org/10.15252/msb.20178126.

25. Collins, B.C., Hunter, C.L., Liu, Y., Schilling, B., Rosenberger, G., Bader, S.L., Chan, D.W., Gibson, B.W., Gingras, A.C., Held, J.M., et al. (2017). Multi-laboratory assessment of reproducibility, qualitative and quantitative performance of SWATH-mass spectrometry. Nat. Commun. *8*, 291. https://doi.org/10.1038/s41467-017-00249-5.

26. Srivastava, P. (2002). Roles of heat-shock proteins in innate and adaptive immunity. Nat. Rev. Immunol. *2*, 185–194. https://doi.org/10.1038/nri749.

27. Ko, E.J., Lee, Y.T., Kim, K.H., Lee, Y., Jung, Y.J., Kim, M.C., Lee, Y.N., Kang, T., and Kang, S.M. (2017). Roles of aluminum hydroxide and monophosphoryl lipid A adjuvants in overcoming CD4+ T cell deficiency to induce isotype-switched IgG antibody responses and protection by T-dependent influenza vaccine. J. Immunol. *198*, 279–291. https://doi.org/10.4049/jimmunol.1600173.

28. Heberle, H., Meirelles, G.V., da Silva, F.R., Telles, G.P., and Minghim, R. (2015). InteractiVenn: a web-based tool for the analysis of sets through Venn diagrams. BMC Bioinformatics *16*, 169. https://doi.org/10.1186/s12859-015-0611-3.

29. Luo, X., Huang, S., Luo, S., Liao, H., Wang, Y., Deng, X., Ma, F., Ma, C.W., and Zhou, L. (2018). Identification of genes underlying the enhancement of immunity by a formula of lentinan, pachymaran and tremelia polysaccharides in immunosuppressive mice. Sci. Rep. *8*, 10082. https://doi.org/10.1038/s41598-018-28414-w.

30. Zhu, W., Lönnblom, E., Förster, M., Johannesson, M., Tao, P., Meng, L., Lu, S., and Holmdahl, R. (2020). Natural polymorphism of Ym1 regulates pneumonitis through alternative activation of macrophages. Sci. Adv. *6*, eaba9337. https://doi.org/10.1126/sciadv.aba9337.

31. Kościuczuk, E.M., Lisowski, P., Jarczak, J., Strzałkowska, N., Jóźwik, A., Horbańczuk, J., Krzyżewski, J., Zwierzchowski, L., and Bagnicka, E. (2012). Cathelicidins: family of antimicrobial peptides. A review. Mol. Biol. Rep. *39*, 10957–10970. https://doi.org/10.1007/s11033-012-1997-x.

32. Moschen, A.R., Adolph, T.E., Gerner, R.R., Wieser, V., and Tilg, H. (2017). Lipocalin-2: a master mediator of intestinal and metabolic inflammation. Trends Endocrinol. Metab. *28*, 388–397. https://doi.org/10.1016/j.tem.2017.01.003.

33. Arthur, J.S.C., and Ley, S.C. (2013). Mitogen-activated protein kinases in innate immunity. Nat. Rev. Immunol. *13*, 679–692. https://doi.org/10.1038/nri3495.

34. Reina, S., Nibali, S.C., Tomasello, M.F., Magrì, A., Messina, A., and De Pinto, V. (2022). Voltage dependent anion channel 3 (VDAC3) protects mitochondria from oxidative stress. Redox Biol. *51*, 102264. https://doi.org/10.1016/j.redox.2022.102264.

35. Elhodaky, M., and Diamond, A.M. (2018). Selenium-binding protein 1 in human health and disease. Int. J. Mol. Sci. *19*, 3437. https://doi.org/10.3390/ijms19113437.

36. Daugaard, M., Rohde, M., and Jäättelä, M. (2007). The heat shock protein 70 family: highly homologous proteins with overlapping and distinct functions. FEBS Lett. *581*, 3702–3710. https://doi.org/10.1016/j.febslet.2007.05.039.

37. Coffman, R.L., Sher, A., and Seder, R.A. (2010). Vaccine adjuvants: putting innate immunity to work. Immunity *33*, 492–503. https://doi.org/10.1016/j.immuni.2010.10.002.

38. Marciani, D.J. (2003). Vaccine adjuvants: role and mechanisms of action in vaccine immunogenicity. Drug Discov. Today *8*, 934–943.

39. Awate, S., Babiuk, L.A., and Mutwiri, G. (2013). Mechanisms of action of adjuvants. Front. Immunol. *4*, 114. https://doi.org/10.3389/fimmu.2013.00114.

40. Wen, Y., and Shi, Y. (2016). Alum: an old dog with new tricks. Emerg. Microbes Infect. *5*, e25. https://doi.org/10.1038/emi.2016.40.

41. Seubert, A., Calabro, S., Santini, L., Galli, B., Genovese, A., Valentini, S., Aprea, S., Colaprico, A., D'Oro, U., Giuliani, M.M., et al. (2011). Adjuvanticity of the oil-in-water emulsion MF59 is independent of Nlrp3 inflammasome but requires the adaptor protein MyD88. Proc. Natl. Acad. Sci. USA *108*, 11169–11174. https://doi.org/10.1073/pnas.1107941108.

42. Casella, C.R., and Mitchell, T.C. (2008). Putting endotoxin to work for us: monophosphoryl lipid A as a safe and effective vaccine adjuvant. Cell. Mol. Life Sci. *65*, 3231–3240. https://doi.org/10.1007/s00018-008-8228-6.

43. Savage, S.R., and Zhang, B. (2020). Using phosphoproteomics data to understand cellular signaling: a comprehensive guide to bioinformatics resources. Clin. Proteomics *17*, 27. https://doi.org/10.1186/s12014-020-09290-x.

44. Timp, W., and Timp, G. (2020). Beyond mass spectrometry, the next step in proteomics. Sci. Adv. *6*, eaax8978. https://doi.org/10.1126/sciadv.aax8978.

45. Fabregat, A., Sidiropoulos, K., Viteri, G., Forner, O., Marin-Garcia, P., Arnau, V., D'Eustachio, P., Stein, L., and Hermjakob, H. (2017). Reactome pathway analysis: a high-performance in-memory approach. BMC Bioinformatics *18*, 142. https://doi.org/10.1186/s12859-017-1559-2.

46. Mi, H., Muruganujan, A., Huang, X., Ebert, D., Mills, C., Guo, X., and Thomas, P.D. (2019). Protocol update for large-scale genome and gene function analysis with the PANTHER classification system (v.14.0). Nat. Protoc. *14*, 703–721. https://doi.org/10.1038/s41596-019-0128-8.

47. Burny, W., Callegaro, A., Bechtold, V., Clement, F., Delhaye, S., Fissette, L., Janssens, M., Leroux-Roels, G., Marchant, A., van den Berg, R.A., et al. (2017). Different adjuvants induce common innate pathways that are associated with enhanced adaptive responses against a model antigen in humans. Front. Immunol. *8*, 943. https://doi.org/10.3389/fimmu.2017.00943.

48. Cottey, R., Rowe, C.A., and Bender, B.S. (2001). Influenza virus. Curr. Protoc. Immunol. Chapter 19, Unit 19.11. https://doi.org/10.1002/0471142735.im1911s42.

49. Jamwal, R., Barlock, B.J., Adusumalli, S., Ogasawara, K., Simons, B.L., and Akhlaghi, F. (2017). Multiplex and label-free relative quantification approach for studying protein Abundance of drug metabolizing enzymes in human liver microsomes using SWATH-MS. J. Proteome Res. *16*, 4134–4143. https://doi.org/10.1021/acs.jproteome.7b00505.

50. Jamwal, R., Topletz, A.R., Ramratnam, B., and Akhlaghi, F. (2017). Ultra-high performance liquid chromatography tandem mass-spectrometry for simple and simultaneous quantification of cannabinoids. J. Chromatogr. B Analyt. Technol. Biomed. Life Sci. *1048*, 10–18. https://doi.org/10.1016/j.jchromb.2017.02.007.

51. Wiśniewski, J.R., and Rakus, D. (2014). Multi-enzyme digestion FASP and the 'total protein approach'-based absolute quantification of the Escherichia coli proteome. J. Proteomics *109*, 322–331. https://doi.org/10.1016/j.jprot.2014.07.012.

52. Pursiheimo, A., Vehmas, A.P., Afzal, S., Suomi, T., Chand, T., Strauss, L., Poutanen, M., Rokka, A., Corthals, G.L., and Elo, L.L. (2015). Optimization of statistical methods impact on quantitative proteomics data. J. Proteome Res. *14*, 4118–4126. https://doi.org/10.1021/acs.jproteome.5b00183.

STAR★METHODS

KEY RESOURCES TABLE

REAGENT or RESOURCE	SOURCE	IDENTIFIER
Antibodies		
HRP-conjugated sheep anti-mouse IgG secondary antibodies	GE Healthcare Life Sciences	NA931; RRID: AB_772210
Bacterial and virus strains		
Influenza A Virus, A/California/07/2009 (H1N1)	International Reagent Resource	FR-201
Mouse-adapted Influenza A Virus, A/California/07/2009 (H1N1)	Cao et al.[7]	N/A
Biological samples		
Recombinant hemagglutinin antigen (rHA) of influenza A/California/07/2009 (H1N1)	International Reagent Resource	FR-559
Monovalent 2009 H1N1 influenza (pdm09) vaccine	BEI Resources	NR-20083
Chicken red blood cells	Charles River Laboratories	10100767
Egg (9–11 days incubated), SPF, Premium, Fertile	Charles River Laboratories	10100332
Receptor-destroying enzyme (RDE)	Hardy Diagnostics	370013
Chemicals, peptides, and recombinant proteins		
TRIzol™ Reagent	Thermo Fisher Scientific	15596026
AddaVax™	InvivoGen	vac-adx-10
Alhydrogel® adjuvant 2%	InvivoGen	vac-alu-250
Endotoxin-free OVA	InvivoGen	vac-pova
Isopropanol	Fisher Scientific	BP2618-500
Chloroform	Fisher Scientific	BP1145-1
Lipid A, monophosphoryl (MPL)	Sigma	L6895
Dithiothreitol (DTT)	Thermo Fisher Scientific	R0862
Iodoacetamide	Sigma	I1149
Ammonium bicarbonate	Sigma	09830
Sodium deoxycholate	Sigma	30970
TPCK-treated trypsin	Sigma	4370285
Gibco™ PBS, pH 7.4	Thermo Fisher Scientific	10010023
Tween 20	Sigma	P1379
TMB substrate	Fisher Scientific	PI34028
Critical commercial assays		
High Capacity cDNA Reverse Transcription Kit	Thermo Fisher Scientific	Cat# 4368814
PowerUp™ SYBR™ Green Master Mix	Thermo Fisher Scientific	Cat# 00868399
Pierce BCA Protein Assay Kit	Thermo Fisher Scientific	Cat# 23227
Deposited data		
Raw proteomics data	MassIVE repository	MSV000090681
Experimental models: Organisms/strains		
C57BL/6 mouse	Charles River Laboratories	N/A
HSP70 KO mouse (cryo-preserved)	Mutant Mouse Resource & Research Centers (MMRRC) at University of Missouri	Cat# 030411-MU

(*Continued on next page*)

Continued

REAGENT or RESOURCE	SOURCE	IDENTIFIER
Oligonucleotides		
Hspa1a forward primer: TGGTGCAGTCCGACATGAAG	This paper	N/A
Hspa1a reverse primer: GCTGAGAGTCGTTGAAGTAGGC	This paper	N/A
Hspa1b forward primer: GAGATCGACTCTCTGTTCGAGG	This paper	N/A
Hspa1b reverse primer: GCCCGTTGAAGAAGTCCTG	This paper	N/A
GAPDH forward primer: AGGTCGGTGTGAACGGATTTG	This paper	N/A
GAPDH reverse primer: TGTAGACCATGTAGTTGAGGTCA	This paper	N/A
Software and algorithms		
Analyst TF	AB Sciex	Version 1.7.1 (2019)
Spectronaut	Biognosys	Ver. 13.10.191212.43655
Reactome (online database)	Fabregat et al.[45]	https://reactome.org/
Panther Classification System (online tool)	Mi et al.[46]	http://pantherdb.org
InteractiVenn (online tool)	Heberle et al.[28]	http://www.interactivenn.net/
GraphPad PRISM	GraphPad Software	Version 9.4.1 (2022)

RESOURCE AVAILABILITY

Lead contact

Further information and requests for resources and reagents should be directed to and will be fulfilled by the lead contact Xinyuan Chen (xchen14@uri.edu).

Materials availability

This study did not generate new unique reagents.

Data and code availability

- Proteomics data have been deposited in MassIVE: MSV000090681 and made publicly accessible.
- This study does not report original code.
- Any additional information required to reanalyze the data reported in this paper is available from the lead contact upon request.

EXPERIMENTAL MODEL AND SUBJECT DETAILS

Mice

Male C57BL/6 mice (6–8 weeks old) were purchased from Charles River Laboratories (Wilmington, MA, USA). HSP70 KO mice (cryo-preserved, 030411-MU) were ordered from Mutant Mouse Resource & Research Centers (MMRRC) at the University of Missouri. One litter of heterologous HSP70 mice were received and self-bred to obtain initial HSP70 WT and HSP70 KO mice for self-breeding to obtain sufficient mice for use in this study. Animals were housed in animal facilities of University of Rhode Island (URI). Anesthesia was induced by intraperitoneal injection of a mixture of Ketamine (80 mg/kg) and Xylazine (10 mg/kg). All animal procedures were approved by the Institutional Animal Care and Use Committee of URI with protocol number AN1516-004.

METHOD DETAILS

RFA treatment

A cosmetic fractional bipolar RF device (Norlanya Technology Co., Hong Kong, China) equipped with 12 × 12 array of microelectrodes in 2 × 2 cm^2 area was used in this study. For RF treatment, a thin layer of ultrasound coupling medium was topically applied followed by firmly pressing the tip of the RF device on skin surface and then holding the device in position for 1–2 min at the high-energy setting (n = 3). Sham treatment followed the same procedures except the device was not activated (n = 4).

Chemical adjuvant treatment

For chemical adjuvant treatment, hair-removed lateral dorsal skin of mice was intradermally injected with 20 μL AddaVax (1:1 vol/vol mixed with phosphate buffered saline (PBS)), Alum (Alhydrogel, 160 μg aluminum hydroxide), MPL (25 μg), or MPL (25 μg)/Alum adjuvant (Alhydrogel, 100 μg aluminum hydroxide) (n = 3). AddaVax was prepared by 1:1 (vol/vol) mixing with PBS. Alum adjuvant was prepared by 4:1 (vol/vol) mixing with PBS. MPL (1 mg) was dissolved in 100 μL DMSO and then mixed with 300 μL endo-free H_2O. Before injection, MPL was mixed with PBS at 1:1 (vol/vol) ratio. MPL/Alum adjuvant was prepared by mixing MPL (2.5 mg/mL) with Alum at 1:1 (vol/vol) ratio to simulate the combinatorial AS04 adjuvant.[47]

Immunization

Hair-removed lateral dorsal skin of mice was exposed to RF or Sham treatment followed by ID injection of 20 μL endo-free OVA (10 μg) or pdm09 vaccine (0.3 μg) into RF or Sham-treated skin under anesthesia. Mice were then recovered on a digitally controlled warm pad.

HI titer

Serum hemagglutination inhibition (HI) titer was measured following a well-established protocol.[48] In detail, serum samples (15 μL) were incubated with 45 μL receptor-destroying enzyme (RDE) II at 37°C overnight followed by heat inactivation at 56°C for 30 min. Serum samples were then incubated with 60 μL chicken RBCs (1% in PBS) at room temperature for 30 min to remove non-specific binding. The tubes were inverted every 10 min to mix the contents. Chicken RBCs were removed by centrifugation at 14,000 rpm for 5 seconds. Supernatants were collected (slightly more than 100 μL) and subjected to a two-fold serial dilution in V-shaped 96-well plates. In brief, 50 μL heat-inactivated, adsorbed serum samples were added to duplicate, adjacent wells in row A and row B with wells from row B to G containing 50 μL PBS/0.5% BSA. Contents in wells of row B were mixed and 50 μL was transferred to succeeding wells of row C and continue the two-fold dilutions through row G. After mixing the contents in wells of row G, 50 μL sample was discarded. Wells in row H were added with 100 μL PBS/0.5% BSA. Four hemagglutinating units of pdm09 viruses (A/California/07/2009) in 50 μL volume were then added to all wells except for row H. Plates were incubated at room temperature for 30 min. After that, 50 μL 1% chicken RBCs were added to all wells. Plates were further incubated at room temperature for 45 min followed by reading agglutination patterns. HI titer was determined as the reciprocal of the highest dilution that completely inhibited agglutination of chicken RBCs.

ELISA antibody titer

Serum antibody titer was measured by enzyme-linked immunosorbent assay (ELISA). In brief, 96-well ELISA plates were coated with 10 μg/mL OVA or 1 μg/mL rHA at 4°C overnight. After blocking with 5% non-fat milk, two-fold serial dilutions of immune sera were added and incubated at room temperature for 90 min. After washing in PBS supplemented with 0.05% Tween 20 (PBST), HRP-conjugated sheep anti-mouse IgG secondary antibodies (1:5,000, NA931, GE Healthcare Life Sciences) were added and incubated at room temperature for 1 h. After washing in PBST, TMB substrates were added and reactions were stopped by addition of 3 M H_2SO_4. Optical absorbance (OD_{450nm}) was read in a microplate reader (Molecular Device). Serum antibody titer was defined as the reciprocal dilution factor that resulted in OD_{450nm} that was ~3 times higher than the background value.

Lethal viral challenge

Mouse-adapted pdm09 viruses were prepared as in our previous report.[7] Mice were intranasally challenged with 10× LD50 pdm09 viruses under light anesthesia. Mouse body weight and survival were monitored daily for 14 days. Mice were euthanized and considered dead if their body weight loss was more than 25%.

Real-time PCR

Tissue RNA was isolated with Trizol™ reagent following manufacturer's instructions. DNase and RNase-free reagents and supplies were used in RNA purification. Mouse skin of ~12 mm × 12 mm was minced into small pieces and then homogenized in 1 mL Trizol™ reagent. Tissue homogenates were centrifuged at 12,000 g at 4°C for 5 min. Supernatants were collected into an Eppendorf tube and incubated at room temperature for 5 min. 0.2 mL chloroform was added and the Eppendorf tube was inverted for several times to mix the contents. After 3 min of incubation at room temperature, samples were centrifuged at 12,000 g at 4°C for 15 min. The top aqueous phase (~300 μL) was transferred to new Eppendorf tubes without disturbing the interface. 0.5 mL isopropanol was added to the aqueous phase and the mixture was incubated at room temperature for 10 min. Eppendorf tubes were centrifuged at 12,000 g at 4°C for 10 min to pellet the RNA. Supernatants were carefully removed and discarded. 1 mL 75% ethanol was added and the tube was inverted multiple times to resuspend the RNA pellets. Tubes were centrifuged at 7,500 g at 4°C for 5 min. Supernatants were carefully removed and discarded. RNA was dried at room temperature for 15–20 min. 40 μL RNase-free water was added and the tube was incubated at 55°C for 15 min. RNA concentration and purity were measured by reading optical density at 260 and 280 nm. RNA quality was evaluated by agarose gel electrophoresis (1% agarose gel).

The same amount (1 μg) of RNA across groups was reverse transcribed with the High Capacity cDNA Reverse Transcription Kit without using RNase inhibitor. In more detail, 2× RT master mix was prepared by mixing 2 μL 10× RT Buffer, 0.8 μL dNTP Mix, 2.0 μL RT Random Primers, 1.0 μL Reverse Transcriptase and 4.2 μL Nuclease-free H_2O per sample. 10 μL RNA (adjusted to the required amount with RNase-free H_2O) was then mixed with 10 μL 2× RT master mix. The mixture was incubated in a thermal cycler with below program: 25°C for 10 min, then 37°C for 120 min, then 85°C for 5 min, and lastly 4°C forever.

For RT-PCR, 0.5 μL cDNA was mixed with 1 μL forward and 1 μL reverse primer of respective genes (sequence see key resources table), 7.5 μL nuclease-free H_2O, and then mixed with 10 μL 2× PowerUp™ SYBR™ Green Master Mix. RT-PCR was conducted in Applied Biosystems ViiA 7 with below PCR program: 50°C for 2 min, then 95°C for 2 min, and then 40 cycles of 95°C for 15 s and then 60°C 1 min. The mRNA levels were normalized with the mRNA levels of GAPDH and analyzed with the $2^{-\Delta\Delta Ct}$ method.

Skin processing for proteomics analysis

Skin was harvested 18 h after adjuvant treatment. Skin was prepared for LC-MS/MS analysis according to a published protocol with slight modifications.[49] In brief, ~60 mg skin was homogenized in 8 M urea (1 mL). After centrifugation, supernatants were collected for quantification of protein concentrations with Pierce BCA Protein Assay Kit. Skin homogenates (~250 μg) were incubated with 25 μL DTT (100 mM) at 35°C for 30 min. Samples were alkylated by incubation with 25 μL iodoacetamide (IAA; 200 mM) at room temperature for 30 min. Proteins were precipitated in cold water, methanol, and chloroform (1:2:1, v/v). Protein pellets were washed with ice-cold methanol and resuspended in 135 μL 50 mM ammonium bicarbonate (pH 8.0) supplemented with 3% w/v sodium deoxycholate. Samples were then digested with TPCK-treated trypsin (12.5 μg) in a Barocycler (NEP2320, Pressure Biosciences Inc., Easton, MA). Following the first run, 12.5 μg trypsin was added and the digestion was repeated in the same condition. After that, 15 μL acetonitrile:water (1:1, v/v) containing 5% formic acid was added. After centrifugation, 80 μL supernatants were collected and 25 μL volume was injected for LC-MS/MS analysis.

LC-MS/MS

Proteomic experiments were conducted in positive ionization mode using a DuoSpray™ ion source on a Sciex 5600 TripleTOF™ mass spectrometer (Sciex, Framingham, MA, USA) coupled to an Acquity UPLC H-Class system (Waters Corp., Milford, MA, USA) for chromatographic separation according to a published protocol with slight modifications.[50] Peptide separation was achieved over 180 min gradient method at 100 μL/min on an Acquity UPLC Peptide BEH C18 column (2.1 × 150 mm, 300 Å, 1.7 μm) preceded with an Acquity VanGuard pre-column (2.1 × 5 mm, 300 Å, 1.7 μm) (Waters Corp., Milford, MA, USA). Mobile phase A was H_2O (0.1% formic acid) and mobile phase B was acetonitrile (0.1% formic acid). Gradient conditions were 98% A from 0 to 5 min, 98 to 70% A from 5 to 155 min, 70 to 50% A from 155 to 160 min, 50 to 5% A from 160 to 170 min, and 5% to 98% A from 170 to 180 min. The gradient was returned to initial conditions at the end of each run to equilibrate the column before the start of the next run. The flow was diverted to waste for the first 5 min and last 10 min of the acquisition. The autosampler was maintained at 10°C and the

column was kept at 50°C. Trypsin-digested β-galactosidase peptides were injected to monitor TOF detector mass calibration after every four samples.

Data was acquired using Analyst TF 1.7.1 software (2019, AB Sciex), followed by data-independent analysis (DIA) as previously described.[49,50] Ion spray voltage floating (ISVF) was kept at 5500 V while the source temperature was set at 500°C. Gas 1 (GS1), gas 2 (GS2), and curtain gas (CUR) were set at 55, 60, and 25 psi, respectively. Declustering potential (DP), collision energy (CE), and collision energy spread (CES) were set at 120, 10, and 5, respectively. During the survey scan, all the ions with a charge state of 2–4, mass range of *m/z* 300–1250, and exceeding 25 cps were used for MS/MS analysis. Former target ions were excluded for 8 s and the mass tolerance for TOF-MS was 50 mDa with a 100 ms accumulation time. For the product scan, data were acquired from 100 to 1250 *m/z* with an accumulation time of 75 ms and a total cycle time of 3.5 s. Production analysis was done under dynamic accumulation and rolling collision energy dependent on the *m/z* of the ion. All the parameters for SWATH-MS data acquisition were similar as described above except the following: source temperature was 400°C, GS1 was 55 psi, and TOF masses were collected from *m/z* 300 to 1500. The total cycle time for SWATH acquisition was 3.95 s. SWATH data was acquired (*m/z* 400–1100) over 70 SWATH windows per cycle with a window size of *m/z* 10.

Data processing

The absolute level of proteins was determined from DIA data handled by Spectronaut (Ver. 13.10.191212.43655, Biognosys, Schlieren, Switzerland) with an internal MDSC spectral library generated by Pulsar (26,184 precursors targeted, 4955 mutated precursors added) and the murine FASTA file from UNIPROT (UP000000589_Mice Reference, release date 8/10/2019, 22,296 protein entries searched). All Spectronaut settings were kept at factory default except "PTM localization" was deselected. Protease specificity was set to Trypsin-P, fixed modification considered was carbamidomethyl, and variable modifications considered were acetyl (protein n-term) and oxidation (M). MS1 and MS2 mass tolerances were set to dynamic with the optimal range determined by Spectronaut. Individual spectra were selected via threshold scoring based on relative ion intensity relative to the most intense (base) peak. False discovery rate (FDR) was set to 0.01 and estimated by Pulsar at the peptide, protein and peptide-spectrum match (PSM) levels. Proteins were then identified and quantified from the DIA data using Spectronaut. Precursor ion detection was performed with extracted ion current chromatogram (XIC) RT, with mass tolerance set to dynamic, and optimally determined by Spectronaut. Precursor identification was based on a q-value (FDR) cut-off of 0.01, and only precursors satisfying this cut-off were accepted. XIC RT window was set to dynamic, with optimal tolerances determined by Spectronaut, and the correction factor set to system default (1, no correction). A maximum of three and a minimum of one peak were considered for identifying peptides, and were selected based on intensity, with selection method set to "maximum intensity" (default setting). All mass tolerances were set to dynamic and optimally determined by Spectronaut. FDR was set to 0.01 and estimated by Pulsar at the peptide, protein and peptide-spectrum match (PSM) levels. FDR was estimated using decoy peptides generated in-silico, as the fraction of decoys in the total identified peptides. Decoy generation method was set to "mutated" (default setting). Protein intensities were normalized by Spectronaut with the normalization strategy set to "Global normalization" (new default setting).

Data analysis

With the output report from Spectronaut, the total number of proteins was obtained by exclusion of 'Filtered' values in each sample and compared among groups. The "Total Protein Approach" was employed for absolute protein level quantitation.[51] In brief, protein amount was calculated from raw intensity values with the formula: $Protein\ (pmol/mg) = \frac{Individual\ protein\ intensity}{Molecule\ weight\ (g/mol) \times Total\ protein\ intensity} \times 10^9$. Student's t-test was then conducted to compare protein amount differences between adjuvant and sham groups by exclusion of 'Filtered' values.[52] Fold change of protein amounts due to adjuvant treatment was also calculated. Volcano plots were prepared based on -log10 (p value) and log2 (fold change) for each adjuvant. Among significantly changed proteins ($p < 0.05$), only proteins with $\geq$30% increase, corresponding to log2 (Fold change) more than 0.378, or $\geq$30% decrease, corresponding to log2 (Fold change) less than −0.514, were considered as differentially expressed proteins (DEPs).

Bioinformatics analysis

Online tool Panther (http://pantherdb.org) was used to analyze functional enrichment for significantly altered proteins fulfilling the 30% change criterion for the different adjuvant groups.[46] A Web-based

tool (InteractiVenn) was used to analyze commonly and differentially induced proteins among the different adjuvant groups.[28] Online tool Reactome (https://reactome.org) was used to analyze biological pathways of DEPs.[45]

QUANTIFICATION AND STATISTICAL ANALYSIS

Data were expressed as mean ± SEM (standard error of the mean). Student's t-test was used to compare differences between groups and one-way ANOVA with Tukey's Multiple Comparison test was used to compare differences for more than 2 groups except otherwise specified. Log-rank (Mantel-Cox) test with Bonferroni correction was used to compare differences of survival between groups. P value was calculated by PRISM software (GraphPad, San Diego, CA) and considered significant if it was less than 0.05.